Materials Advances

ROYAL SOCIETY OF CHEMISTRY

PAPER

View Article Online
View Journal | View Issue

Cite this: *Mater. Adv.*, 2020, **1**, 2862

Tris(triazolo)triazine-based emitters for solution-processed blue thermally activated delayed fluorescence organic light-emitting diodes†‡

Fabian Hundemer, §[a] Ettore Crovini,§[b] Yoshimasa Wada,[c] Hironori Kaji, *[c] Stefan Bräse*[ad] and Eli Zysman-Colman *[b]

Received 31st August 2020,
Accepted 13th October 2020

DOI: 10.1039/d0ma00659a

rsc.li/materials-advances

We report a new emitter **3,4,5-3TCz-TTT** based on a tris(triazolo)triazine acceptor that shows thermally activated delayed fluorescence and cross-compare its performance with the recently reported analogue, **3DMAC-TTT**. These compounds show blue emission and delayed fluorescence with delayed lifetimes on the order of milliseconds. Solution-processed organic light-emitting diodes achieving maximum external quantum efficiencies, EQE_{max}, of 5.8% for **3,4,5-3TCz-TTT** and 11.0% for **3DMAC-TTT**.

Introduction

Organic light-emitting diodes (OLEDs) generate light by the recombination of electrically generated holes and electrons to form excitons that subsequently radiatively decay. Due to spin-statistics, 75% of the generated excitons are triplets, while 25% are singlet excitons.[1,2] Thermally activated delayed fluorescence (TADF) is considered one of the most promising mechanisms for efficient electroluminescent devices[2–5] as 100% of the excitons can be converted to light. A small energy gap between the lowest singlet (S_1) and triplet (T_1) excited states (ΔE_{ST}) enables triplet excitons to be converted to singlet excitons by reverse intersystem crossing (RISC) at ambient temperatures, which can subsequently relax *via* the fluorescence channel. Typically, a small ΔE_{ST} is achieved by the spatial separation of the highest occupied molecular orbital (HOMO) and the lowest unoccupied molecular orbital (LUMO). The classic design strategies are based on the combination of donor and acceptor groups and their small electronic coupling either *via* (1) a twisted intramolecular charge transfer[6–11] transition, (2) a through-space charge-transfer transition,[7,8,12] (3) a spiro-conjugation charge transfer transition[13,14] or (4) an alternating HOMO/LUMO distribution in p,n-doped polycyclic aromatic hydrocarbons, termed a multi-resonance TADF transition.[2,15–18]

By employing solution-based processing techniques,[19–21] large-area OLEDs becomes simpler and more cost-efficient to fabricate. However, solution-processed devices often show inferior performance compared to the vacuum-deposited counterparts.[22–25] For solution-processed devices to become competitive, their performance must improve to rival vacuum-sublimed devices. Typically, solution-processed devices rely on polymer emitters as the use of polymers produces high-quality, defect-free amorphous films. TADF polymers have shown promise as emitters in solution-processed devices.[23,26–28] However, the synthesis of polymers will lead to a mixture of compounds with different molecular weight, each of which will have a slightly different set of photophysical properties that will result in a broadened emission spectrum.[29] Moreover, the photophysical properties of TADF polymers usually suffer due to quenching *via* intra- and inter-molecular charge transfer between the TADF units on the polymer.[30,31] Dendrimeric TADF emitters also show good solubility and generate high-quality amorphous films. OLED performance, however, tends to fall off rapidly with increasing generation size of the dendron and thus far OLEDs using dendrimer emitters have underperformed compared to their polymer and small molecule emitter counterparts.[32] The use of small molecule emitters has to date produced the highest performance solution-processed OLEDs.

[a] *Institute of Organic Chemistry, Karlsruhe Institute of Technology (KIT), Fritz-Haber-Weg 6, 76131 Karlsruhe, Germany. E-mail: braese@kit.edu; Fax: (+49)-721-6084-8581; Tel: (+49)-721-6084-2903*
[b] *Organic Semiconductor Centre, EaStCHEM School of Chemistry, University of St Andrews, St Andrews, Fife, KY16 9ST, UK E-mail: eli.zysman-colman@st-andrews.ac.uk; Web: http://www.zysman-colman.com; Tel: +44 (0)1334 463826*
[c] *Institute for Chemical Research Kyoto University Uji, Kyoto 611-0011, Japan. E-mail: kaji@scl.kyoto-u.ac.jp*
[d] *Institute of Biological and Chemical Systems – Functional Molecular Systems (IBCS-FMS), Karlsruhe Institute of Technology (KIT), Hermann-von-Helmholtz-Platz 1, D-76344, Eggenstein-Leopoldshafen, Germany*

† The research data supporting this publication can be accessed at https://doi.org/10.17630/586490c1-7c86-48aa-ad7c-f90809626afb.

‡ Electronic supplementary information (ESI) available. See DOI: 10.1039/d0ma00659a

§ Equal contributions.

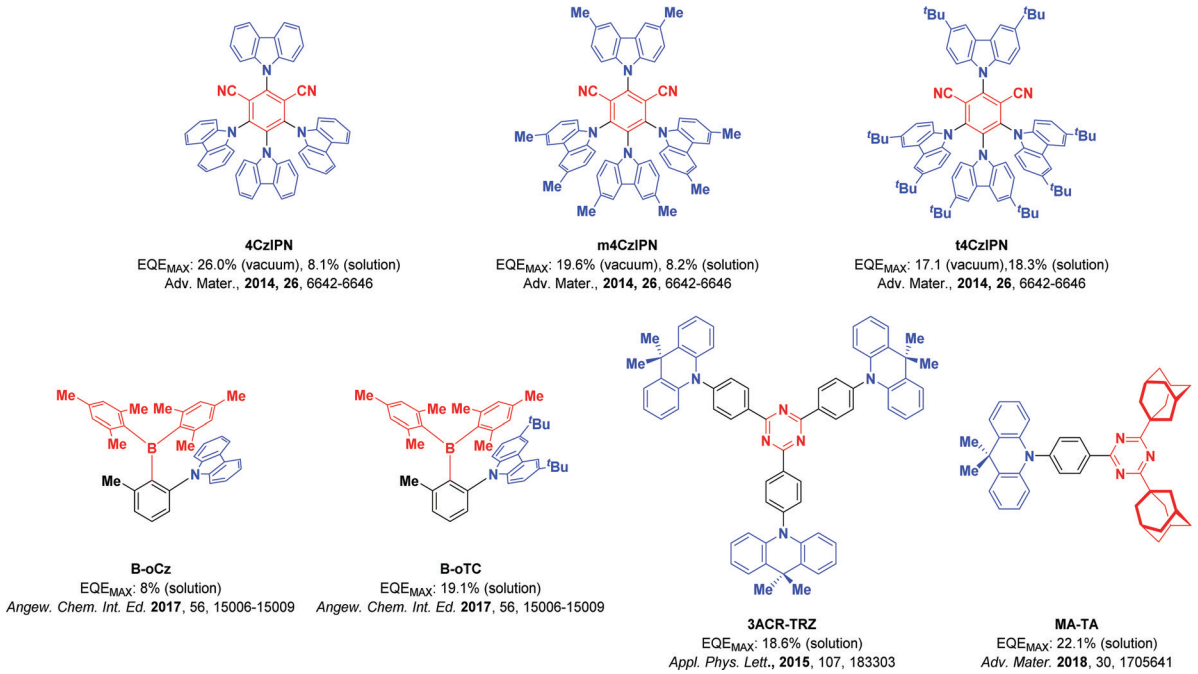

Fig. 1 Molecular structures and performances of the discussed solution-processed materials.

Typically, solubilizing groups are decorated around a known emitter core to improve the film morphology of the emissive layer in solution-processed OLEDs. An example of this can be found in the work of Cho *et al.* where they investigated the effect that solution-processing and vacuum deposition have on the performance of OLEDs, employing three related TADF emitters: **4CzIPN**, **m4CzIPN** and **t4CzIPN** (Fig. 1).[33] The solution-processed device of **4CzIPN** shows a substantial drop in performance compared to the vacuum-deposited OLED (maximum external quantum efficiency, EQE_{max}, decreasing 26.0% to 8.1%). The incorporation of methyl groups in **m4CzIPN** has no effect on the efficiency of the solution-processed device, leading again to inferior efficiencies than the evaporated OLED (from 19.6% to 8.2%). By contrast, the use of *tert*-butylcarbazole in **t4CzIPN** resulted in a much-enhanced solubility of the emitter, stabilizing the morphology of the solution-processed film, which translated into a solution-processed OLED with comparable efficiency to the vacuum-deposited device (17.1% for the vacuum-deposited device and 18.3% for the solution-processed device). In a similar vein, Chen *et al.* reported that the device efficiency could be significantly improved from 8.0% to 19.1% by replacement of carbazole with *tert*-butycarbazole in triarylborane-based TADF emitters.[34] Acridine-based emitters have also been successfully employed in several solution-processed devices. For instance, Wada *et al.* reported a solution-processed OLED using triazine-based TADF emitter **3ACR-TRZ**, which showed an EQE_{max} of 18.6%.[35] The same group reported a high-performance solution-processed blue OLED (CIE: 0.15, 0.19) using **MA-TA** as the emitter, which achieved an EQE_{max} of 22.1%.[36]

1,2,4-Triazoles[37] and 1,3,5-triazines[2,38] have been widely applied as acceptor motifs in TADF materials due to their relatively weak electron-withdrawing character (the LUMO levels are 0.43 eV for 4*H*-1,2,4-triazole and −1.80 eV for 2,4,6-triphenyl-1,3,5-triazine).[39] The combination of these two motifs into a single acceptor in the [1,2,4]-triazolo-[1,3,5]-triazine core (TTT) was synthesized by annulation of three triazole heterocycles onto a central triazine. This motif was first reported in 1911 by Hofmann and Erhardt,[40,41] while Wystrach and co-workers investigated the structure of a triamine TTT derivative in 1953.[42] Then, in 1961, Huisgen *et al.* were the first to synthesize the first TTT core substituted with phenyl groups by reacting cyanuric chloride with 5-phenyl tetrazole.[43] In 2008, Longo *et al.* substituted the TTT core with peripheral flexible alkyl chains, endowing the molecule with liquid crystalline character.[44] The disc-like core with the peripheral aliphatic side chains led to luminescent and charge-transporting materials known to self-assemble into columnar superstructures driven by π-stacking.

Concurrent with our work, Pathak *et al.* recently reported the first two examples of emitters employing the TTT motif within a TADF emitter design: **TTT-PXZ** and **TTT-DMAC** (Fig. 2).[45] These emitters possess moderate photoluminescence quantum yields (Φ_{PL}) of 39.5% and 21.4%, respectively, accompanied by short delayed fluorescence lifetimes of 4.2 μs and 4.6 μs, respectively. The emission of **TTT-PXZ** is expectedly considerably red-shifted given the stronger donor employed, with a λ_{PL} of 522 nm compared to 468 nm for **TTT-DMAC**. The improved device performance of **TTT-PXZ** is in part due to the smaller ΔE_{ST} 0.07 eV compared to 0.20 eV for **TTT-DMAC**. Unfortunately, the devices in this study were poor with EQE_{max} of 6.2 and 1.9% for the OLEDs with **TTT-PXZ** and **TTT-DMAC**, respectively, and associated severe efficiency roll-off.

Wang *et al.*[46] expanded upon this work by improving the efficiency of the DMAC-based OLED (they named the TADF

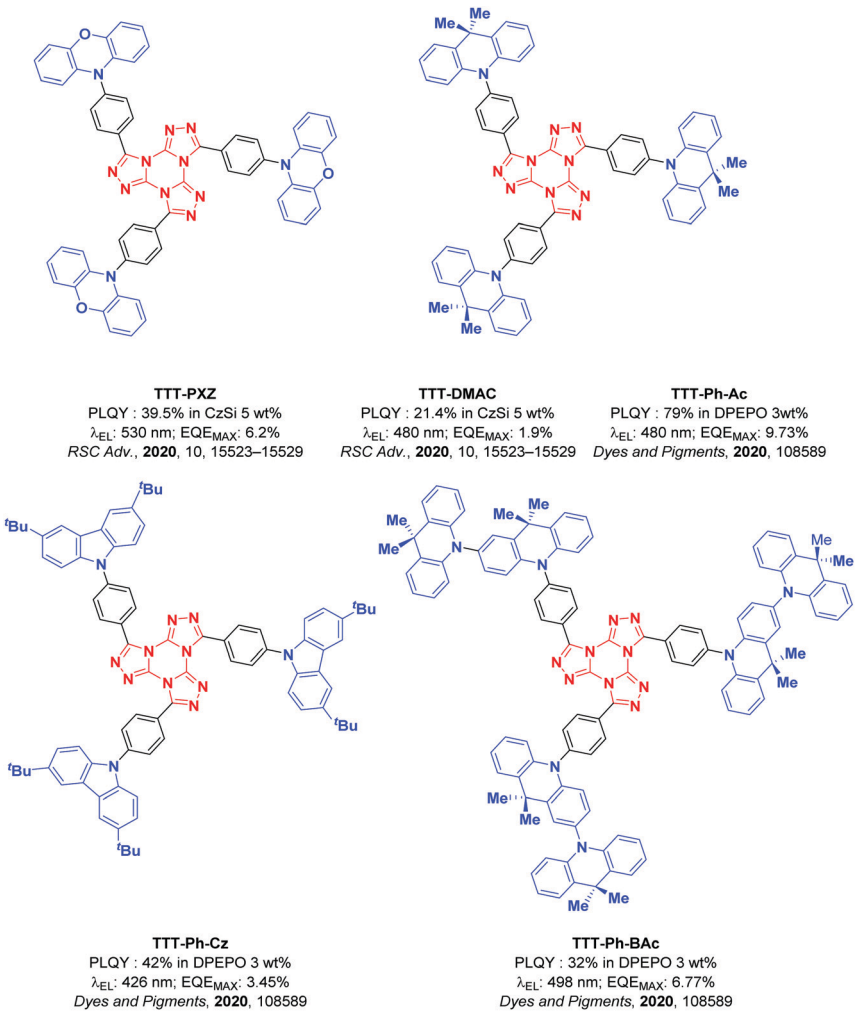

Fig. 2 Molecular structure and OLED performance metrics of known **TTT** emitters.

emitter as **TTT-Ph-Ac** in their work) to 9.73%. They also introduced two new TTT-based emitters: **TTT-Ph-Cz** and **TTT-Ph-BAc** (Fig. 2). **TTT-Ph-Cz** did not present a delayed component, reflected in the low EQE_{max}. **TTT-Ph-BAc** shows a delayed lifetime of 50.7 μs, but the Φ_{PL} is significantly lower at 32%, which translated to a lower EQE_{max} for the OLED using this emitter than in the device using **TTT-Ph-Ac**.

Here, we introduce a new TTT-based emitter (Fig. 3), **3,4,5-3TCz-TTT**, and cross-compare its performance with the recently reported compound **3DMAC-TTT** (aka **TTT-DMAC/TTT-Ph-Ac**).

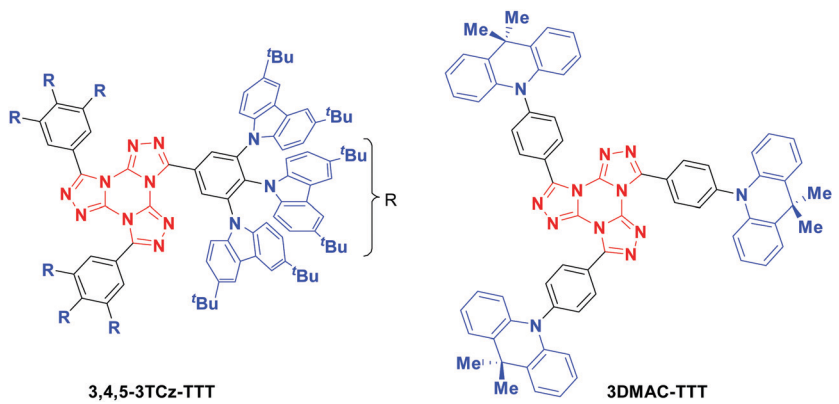

Fig. 3 Molecular structures of **3,4,5-3TCz-TTT** and **3DMAC-TTT**.

Synthesis

The synthesis for the two emitters is shown in Scheme 1. Starting from the 4-fluorobenzonitrile precursors, the DMAC and *tert*-butylcarbazole (TCz) donor groups were attached under basic S_NAr conditions. A 1,3-dipolar cycloaddition reaction with sodium azide and ammonium chloride in DMF at elevated temperatures led to the tetrazole precursors. Following a slightly modified procedure to the literature,[43,47] the TTT core was assembled through a condensation between trichlorotriazine and three equivalents of the tetrazole, yielding **3DMAC-TTT** and **3,4,5-3TCz-TTT** in very good yields. The identity and purity of the two emitters were determined by ^{1}H NMR, ^{13}C NMR, Elemental Analysis (EA) and High-Resolution Mass Spectrometry (HRMS).

Theoretical calculations

To assess the optoelectronic properties of these two compounds, we performed a combination of Density Functional Theory (DFT) calculation and Time-Dependent DFT within the Tamm–Dancoff approximation (TDA-DFT[48]) in the gas phase using the PBE0 functional[49] and the 6-31G(d,p) basis set.[50] These calculations permitted an assessment of the energies and electron density distributions of the frontier molecular orbitals and the nature and energies of the lowest-lying singlet and triplet excited states (Fig. 4). The ground-state optimization of **3,4,5-3TCz-TTT** did not converge due to the large size of the molecule given a large number of *tert*-butyl groups and we thus instead modelled a methyl-substituted analogue (**3,4,5-3MCz-TTT**), which we hypothesized would present the same electronic structure. The calculated HOMO and LUMO values for **3,4,5-3MCz-TTT** are −5.39 eV and −2.14 eV, respectively, while those of **3DMAC-TTT** are −5.39 eV and −1.93 eV, respectively. The different LUMO levels, despite the same acceptor, reflect the different extent of the conjugation present across the TTT core that is governed by the relative sterics of the donor groups. The ΔE_{ST} for **3,4,5-3MCz-TTT** is 0.16 eV while for **3DMAC-TTT** it is 0.01 eV, reflecting the more orthogonal conformation of the donor with respect to the phenylene bridge (DFT calculated torsions are 57.1° for **3,4,5-3TCz-TTT** *versus* 99.5° for **3DMAC-TTT**). Given the presence of three donor groups about the central TTT core, there is significant degeneracy of the low-lying triplet states. For **3,4,5-3MCz-TTT** we can also observe the presence of 5 other intermediate triplet states below the S_1 level, where T_1, T_2, T_3 and T_4, T_5, T_6 each have almost identical energies. The large density of triplet states is a desirable trait that can facilitate RISC.[51–54] For **3DMAC-TTT**, there are three degenerate triplet states present. The oscillator strength (*f*) values for the associated CT transitions from the S_1 state vary markedly at 0.1 and 0.0014 for **3,4,5-3MCz-TTT** and **3DMAC-TTT**, respectively.

Optoelectronic properties

The electrochemistry of the two emitters was studied in degassed acetonitrile (Fig. 5). The CV of **3,4,5-3TCz-TTT** presents three irreversible oxidation waves at 1.15 V, 1.34 V, 1.51 V *vs.* SCE (peaks from DPV), which are assigned to the sequential oxidation of the three TCz groups on each of the arms of the TTT core, values in line for the oxidation potentials of DTCz-containing compounds.[55–59] **3DMAC-TTT** shows one irreversible anodic oxidation wave at 0.91 V *vs.* SCE; the value reported in the literature is 1.15 V *vs.* Fc/Fc^+ in MeCN.[45] Both emitters present a weak reduction wave at −1.76 V and −1.90 V for **3,4,5-3TCz-TTT** and **3DMAC-TTT**, respectively, assigned to the TTT core. The corresponding HOMO and LUMO values for **3,4,5-3TCz-TTT** and **3DMAC-TTT** are −5.57 eV, −2.66 eV and −5.33 eV, −2.52 eV, respectively.

The UV-vis absorption spectrum in DCM (Fig. S23, ESI‡) for **3DMAC-TTT** coincides with the one measured by Pathak *et al.*[45] Both molecules present a low intensity, low energy absorption band around 370 nm that is assigned to an ICT transition from the donor groups to the TTT acceptor. The band at 290 nm is a π–π* locally excited (LE) transition of the DMAC donor. There are four additional absorption bands for **3,4,5-3TCz-TTT** which, by TD-DFT analysis, are assigned to different charge transfer states involving the carbazoles and the bridging phenyl. The absorption spectra for both compounds are not affected by changes in solvent polarity (Fig. 6). By contrast, the broad and unstructured emission red-shifts with increasing solvent polarity, indicating an emissive state that is charge-transfer in nature.

A comparison of the excitation and steady-state emission spectra of the two emitters in DCM is shown in Fig. 6a. Due to the use of stronger DMAC donors, the emission of **3DMAC-TTT**

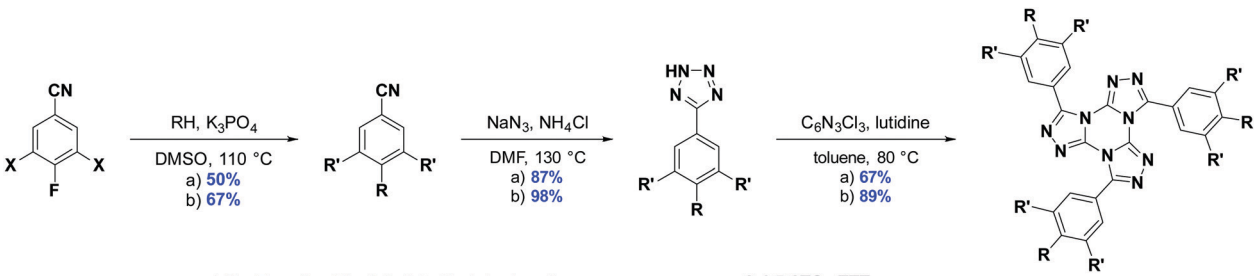

Scheme 1 Synthetic route to **3,4,5-3TCz-TTT** and **3DMAC-TTT**.

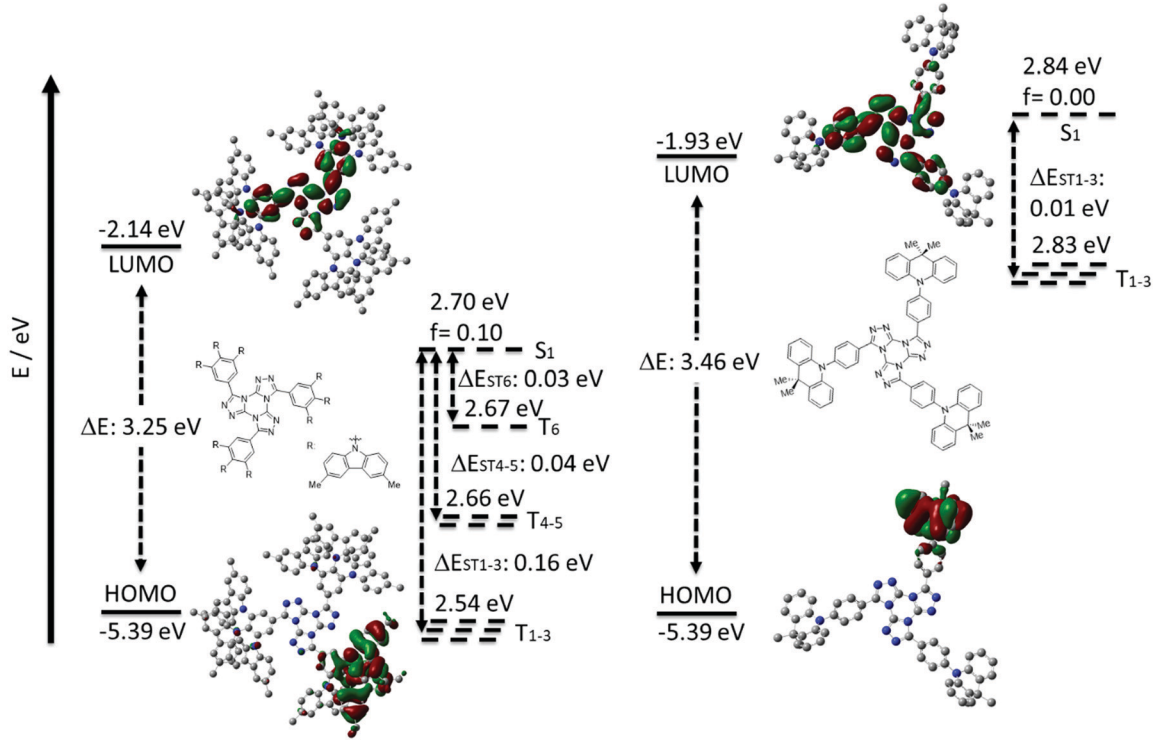

Fig. 4 HOMO and LUMO electron density distributions and energy levels (in eV), excited state energy levels (in eV) **3,4,5-3MCz-TTT** (right) and **3DMAC-TTT** (left) (PBE0/6-31G(d,p)).

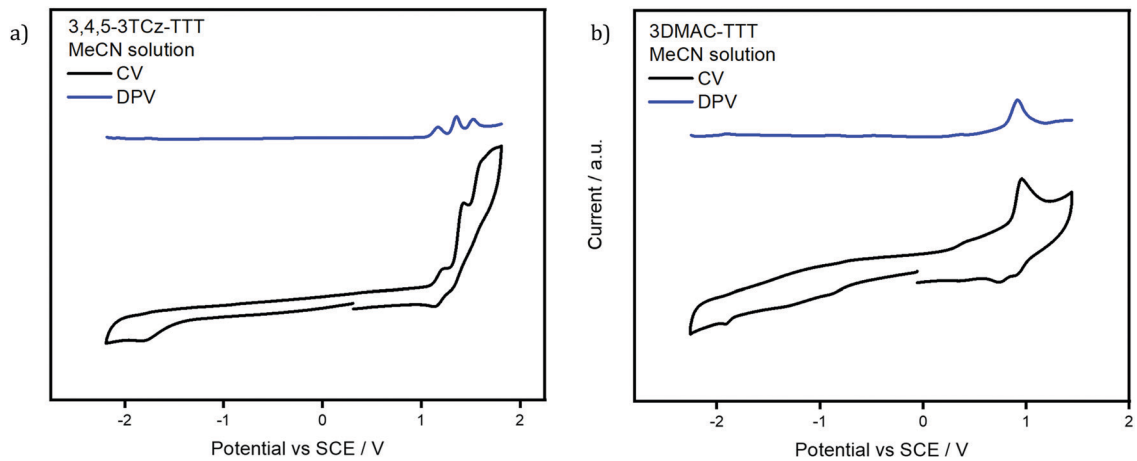

Fig. 5 Cyclic voltammogramn (CV) and differential pulse voltammogram (DPV) of (a) **3,4,5-3TCz-TTT** and (b) **3DMAC-TTT** *versus* saturated calomel electrode (SCE) in MeCN and (scan rate: 0.1 V s^{-1}).

with λ_{PL} at 551 nm is red-shifted compared to that of **3,4,5-3TCz-TTT** (λ_{PL} = 516 nm); the excitation spectra mirror the corresponding absorption spectra. The time-resolved PL decays in degassed DCM are shown in Fig. 7b. Both compounds show mono-exponential decay kinetics (Fig. S25a, ESI‡) with prompt lifetimes, τ_p, of 21.8 ns and 21.6 ns for **3,4,5-3TCz-TTT** and **3DMAC-TTT**, respectively, and delayed lifetimes, τ_d, of 89.7 μs for **3,4,5-3TCz-TTT** and 3.6 μs for **3DMAC-TTT**. Upon exposure to air, the delayed emission was completely suppressed, which is evidence of accessible triplet states that are quenched by oxygen (Tables 1 and 2).

We next identified CzSi as an appropriate host matrix for OLEDs based on its high triplet energy of 3.02 eV.[2] A doping concentration of 15 wt% was chosen as Φ_{PL} was highest (Table S6, ESI‡). Both compounds present sky-blue emission, at 485 nm and 475 nm (Fig. 8b) and high Φ_{PL} under N_2 of 80% and 79% for **3,4,5-3TCz-TTT** and **3DMAC-TTT**, respectively. Both emitters present prompt fluorescence (Fig. S25b, ESI‡),

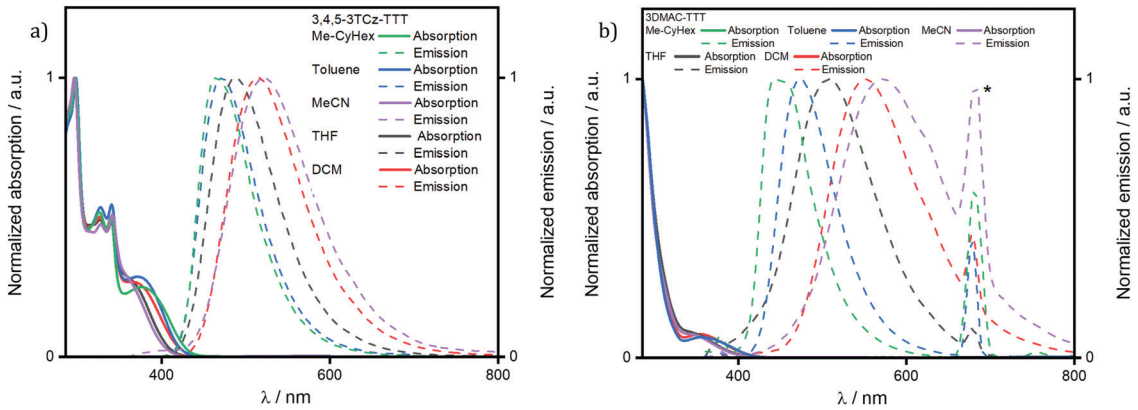

Fig. 6 Solvatochromism study of (a) **3,4,5-3TCz-TTT** and (b) **3DMAC-TTT**. (λ_{exc} = 340 nm. * = second harmonic band of the excitation source).

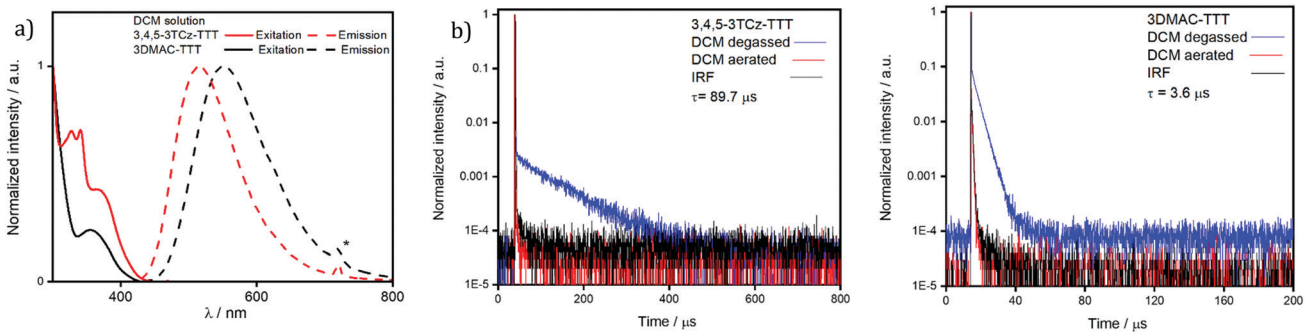

Fig. 7 (a) Emission and excitation spectra of **3,4,5-3TCz-TTT** and **3DMAC-TTT** (DCM 10^{-5} M solutions, λ_{exc} = 360 nm, * = second harmonic of the excitation source). Time-resolved spectroscopy of degassed and aerated solutions of (b) **3,4,5-3TCz-TTT** and (c) **3DMAC-TTT** (DCM 10^{-5} M solutions, λ_{exc} = 378 nm).

Table 1 Solution-state photophysical data

Compound	λ_{PL}[a]/nm	Φ_{PL}[b]/%	E_{gap}[c]/eV	τ_p, τ_d[d]/ns; μs	HOMO[e]/eV	LUMO[e]/eV
3,4,5-3TCz-TTT	516	23	2.88	21.8; 89.7	−5.57	−2.66
3DMAC-TTT	551	13	3.01	21.6; 3.6	−5.33	−2.52

[a] In degassed 10^{-5} M DCM solution. [b] Obtained *via* the relative method (see ESI), quinine sulfate in H_2SO_4 (aq) was used as the reference (Φ_r = 54.6%),[60] λ_{exc} = 360 nm. [c] Obtained from the intersection of the normalized absorption and emission spectra in DCM. [d] τ_p (prompt lifetime) and τ_d (delayed lifetime) were obtained from the transient PL decay of **3,4,5-3TCz-TTT** and **3DMAC-TTT** in DCM. [e] HOMO and LUMO were obtained from the redox potentials from the DPV, $E_{HOMO/LUMO} = -(E_{ox/red} + 4.8)$ where $E_{ox/red}$ were taken from DPV scan corrected *vs.* Fc/Fc$^+$.

with similar lifetimes reflecting tri-exponential decay kinetics, of 14.5 ns [τ_1 = 26.14 ns (12.35%), τ_2 = 12.97 ns (63.43%), τ_3 = 22.71 (24.22%)] for **3,4,5-3TCz-TTT** and bi-exponential decay kinetics 11.9 ns [τ_1 = 6.95 ns (34.7%), τ_2 = 14.6 (65.3%)] for **3-DMAC-TTT**. Both compounds also show very long delayed PL with bi-exponential decay kinetics and lifetimes of 3.1 ms [τ_1 = 1.17 ms (54.27%), τ_2 = 5.30 ms (45.73%)] for **3,4,5-3TCz-TTT** and 4.7 ms [τ_1 = 1.16 ms (46.84%), τ_2 = 7.84 ms (53.16%)] for **3-DMAC-TTT** (Fig. 8a). After investigation at longer time-windows compared to the reference paper,[45] we found that the two emitters present delayed fluorescence with lifetimes of the order of milliseconds, which is the result of

Table 2 Photophysical properties of 15 wt% **3,4,5-3TCz-TTT** and **3DMAC-TTT** doped films in CzSi

Compound	λ_{PL}[a]/nm	Φ_{PL} air; N_2[b]/%	τ_p, τ_d[c]/ns; ms	S_1[d]/eV	T_1[e]/eV	ΔE_{ST}[f]/eV
3,4,5-3TCz-TTT	485	47; 80	14.5; 3.1	2.91	2.70	0.21
3DMAC-TTT	475	28; 79	11.9; 4.7	2.92	2.65	0.27

[a] Measured at room temperature. [b] λ_{exc} = 340 nm. [c] τ_p (prompt lifetime) and τ_d (delayed lifetime) were obtained from the transient PL decay of doped film, λ_{exc} = 378 nm. [d] S_1 was obtained from the onset of the prompt emission measured at 77 K, λ_{exc} = 343 nm. [e] T_1 was obtained from the onset of the phosphorescence spectra measured at 77 K, λ_{exc} = 343 nm. [f] Obtained from the difference of S_1 and T_1.

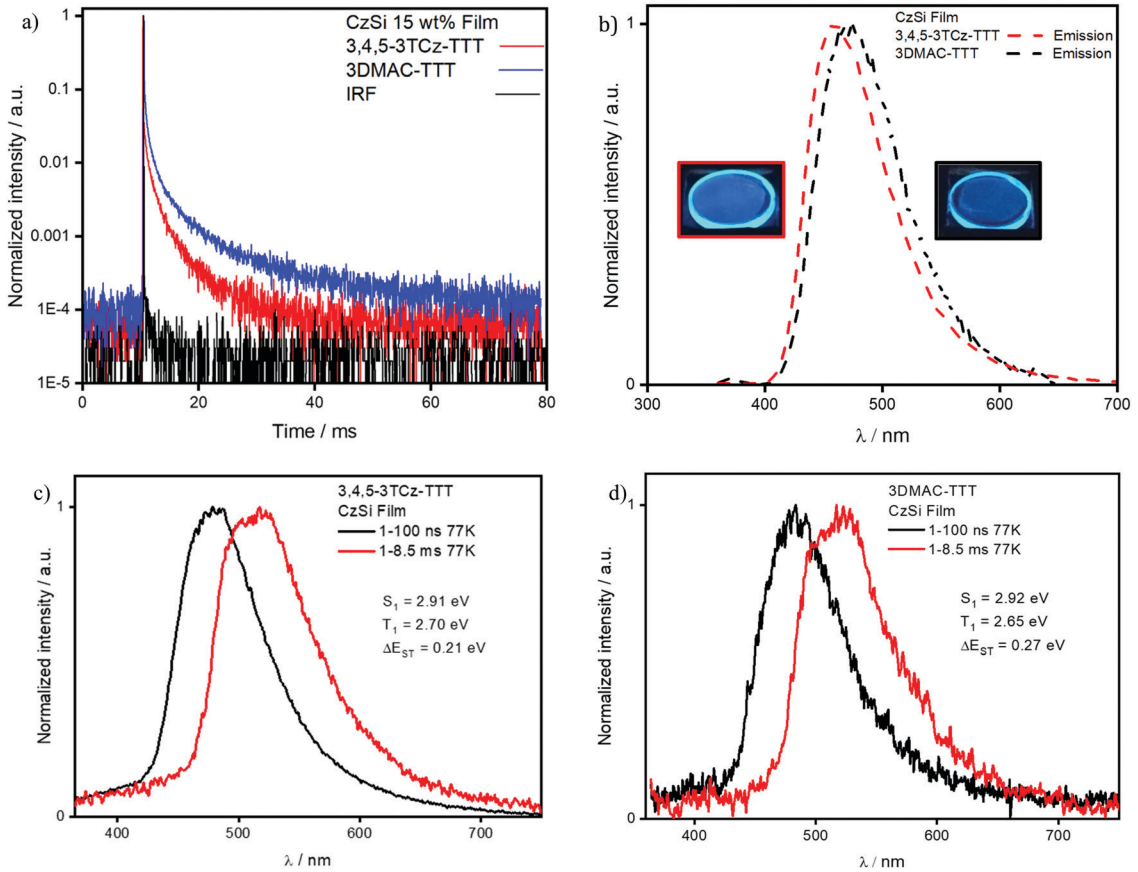

Fig. 8 (a) Time-resolved PL decay of **3,4,5-3TCz-TTT** and **3DMAC-TTT** in spin-coated CzSi film (15 wt%); (b) emission spectra of **3,4,5-3TCz-TTT** and **3DMAC-TTT** in CzSi doped film (15 wt%) (λ_{exc} = 340 nm); prompt fluorescence spectra at 77 K, and phosphorescence spectra at 77 K in 15 wt% CzSi of (c) **3,4,5-3TCz-TTT** and (d) **3DMAC-TTT**, phosphorescence obtained at 77 K at a delay of 1 ms for 8.5 ms, λ_{exc} = 343 nm.

suppression of non-radiative decay in the film, compared to solution and is reflective also in the enhanced photoluminescence quantum yield in the film. Temperature-dependent time-resolved decay curves (Fig. 9) reveal the increase in the intensity of the delayed emission with increasing temperature, which is a hallmark of compounds showing TADF. The ΔE_{ST} values of 0.21 eV for **3,4,5-3TCz-TTT** and 0.27 eV for **3DMAC-TTT** were determined from the onset of the prompt fluorescence and phosphorescence spectra on the CzSi films measured at 77 K (Fig. 8c and d). The latter result is slightly higher compared to that measured by Pathak *et al.*[45] (ΔE_{ST} = 0.20 eV) in the same host matrix.

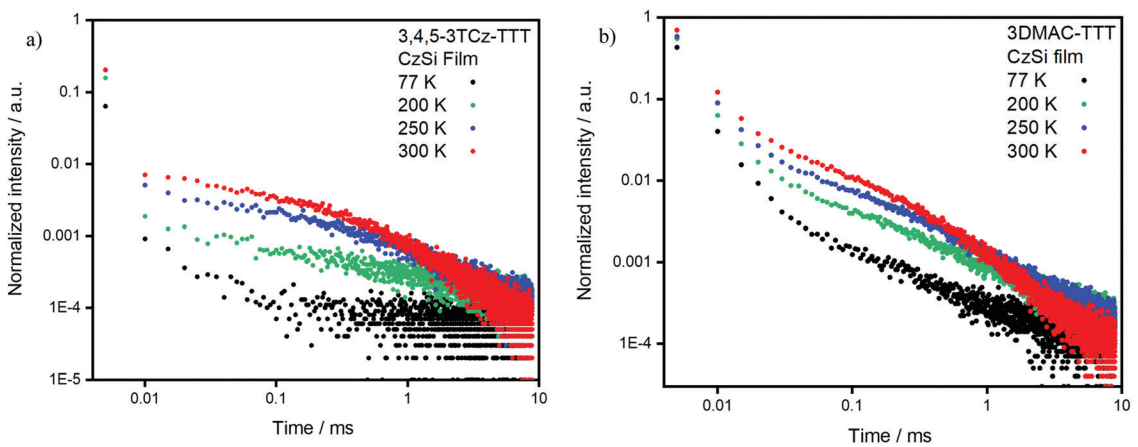

Fig. 9 (a) **3,4,5-3TCz-TTT** and (b) **3DMAC-TTT** delayed fluorescent decay data measured at different temperatures in 15 wt% doped CzSi film (λ_{exc} = 378 nm).

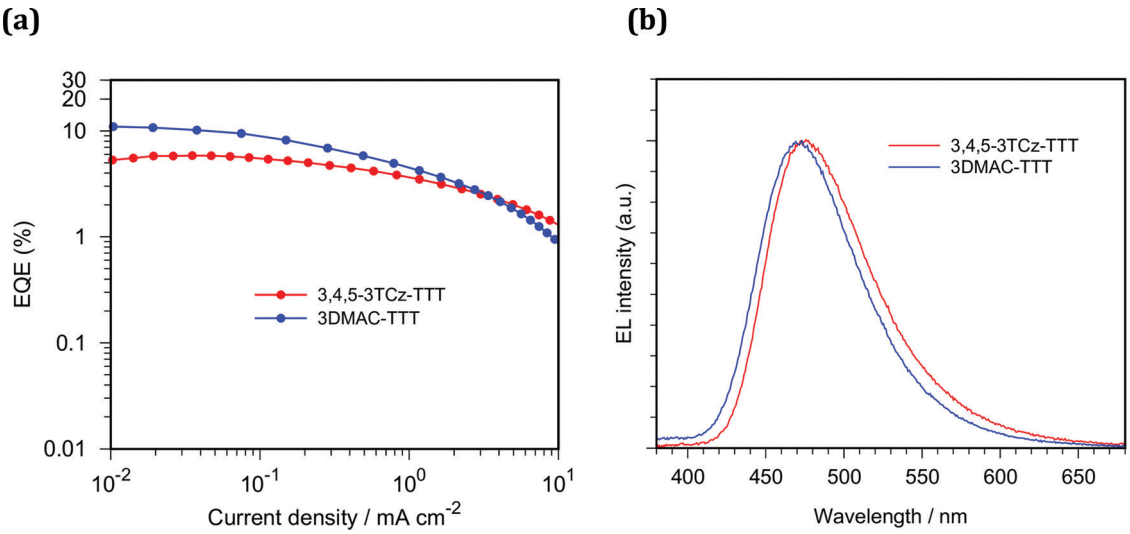

Fig. 10 (a) EQE-current-density characteristics and (b) EL spectra of OLEDs at the current density of 1 mA cm^{-2}. Performances of OLEDs containing **3,4,5-3TCz-TTT** and **3DMAC-TTT** as emitters are displayed in red and blue, respectively.

Solution-processed organic light-emitting diodes

We fabricated solution-processed OLEDs using **3,4,5-3TCz-TTT** and **3DMAC-TTT** as emitters. The device structures consist of: indium tin oxide (ITO)/poly(3,4-ethylenedioxythiophene)–poly (styrenesulfonate) (PEDOT:PSS)/poly(9-vinylcarbazole) (PVK)/15 wt% Emitter:CzSi/dibenzo[*b*,*d*]furan-2,8-diylbis(diphenylphosphine oxide) (PPF)/1,3,5-tris(1-phenyl-1*H*-benzo[*d*]imidazol-2-yl)benzene (TPBi)/lithium quinolin-8-olate (Liq)/Al. PEDOT:PSS, PVK and emitter layers were each deposited by spin-coating and other layers were vacuum-deposited. Here, we inserted the PVK layer to prevent electron leakage from the emitter layer into PEDOT:PSS layer and to confine triplet exciton within the emitter layer. **3,4,5-3TCz-TTT** and **3DMAC-TTT** exhibited blue emission with CIE coordinates of (0.17, 0.28) and (0.16, 0.23) and EQE_{max} of 5.8% and 11.0%, respectively (Fig. 10). Compared to the reported work,[45] **3DMAC-TTT**-based OLED exhibited improved EQE_{max} where the same CzSi host was used. This is probably because better exciton confinement within emitter layer was achieved by inserting PVK layer. Unfortunately, **3,4,5-3TCz-TTT** exhibited lower EQE than that of 3DMAC-TTT, although the device structures are the same. As shown in Fig. S26 (ESI‡), different current density–voltage characteristics were observed, which can be attributed to the different carrier transporting and/or recombination behavior of emitters. From the PLQY and PL lifetime measurements, higher EQE for **3,4,5-3TCz-TTT** OLEDs can be expected when the device structure is further optimized.

Conclusions

We report two examples of TADF molecules using the TTT as a central acceptor. The two compounds emit in the blue and show a long-lived delayed fluorescence with similar lifetimes of 3.1 ms for the **TCz**-based emitter and 4.7 ms for the **DMAC**-containing emitter in CzSi. High photoluminescence quantum yield values of 80% and 79% were observed in CzSi for **3,4,5-3TCz-TTT** and **3DMAC-TTT**, respectively. Both emitters were thus used in solution-processed OLEDs, showing EQE_{max} of 5.8% and 11% for the **3,4,5TCz-TTT** and **3DMAC-TTT** based-devices, respectively. The performance of the **3DMAC-TTT** based is improved compared to previous reports owing to improved exciton management.

Conflicts of interest

There are no conflicts to declare.

Acknowledgements

The KIT authors are part of the Cluster 3D Matter Made To Order under Germany's Excellence Strategy (3DMM2O-EXC-2082-390761711), which has been funded by the German Research Foundation. This work was supported, in part, by the Cooperative Research Center (Sonderforschungsbereich SFB 1176) ''Molecular Structuring of Soft Matter''. This work was partly supported by JSPS KAKENHI grant no. 17H01231 and 17J09631, and by the International Joint Usage/Research Centre (iJURC) at the Institute for Chemical Research (ICR), Kyoto University, Japan. The St Andrews authors thank EU Horizon 2020 Grant Agreement No. 812872 (TADFlife) for funding. EZ-C acknowledges the International Collaborative Research Program of iJURC/ICR, Kyoto University (Grant No. 2020-37).

References

1 M. A. Baldo, D. F. O'Brien, Y. You, A. Shoustikov, S. Sibley, M. E. Thompson and S. R. Forrest, *Nature*, 1998, **395**, 151–154.

2 M. Y. Wong and E. Zysman-Colman, *Adv. Mater.*, 2017, **29**, 1605444.
3 X. Cai and S. J. Su, *Adv. Funct. Mater.*, 2018, **28**, 1–33.
4 Y. Tao, K. Yuan, T. Chen, P. Xu, H. Li, R. Chen, C. Zheng, L. Zhang and W. Huang, *Adv. Mater.*, 2014, **26**, 7931–7958.
5 Y. Liu, C. Li, Z. Ren, S. Yan and M. R. Bryce, *Nat. Rev. Mater.*, 2018, **3**, 18020.
6 G. Méhes, H. Nomura, Q. Zhang, T. Nakagawa and C. Adachi, *Angew. Chem., Int. Ed.*, 2012, **51**, 11311–11315.
7 K. Kawasumi, T. Wu, T. Zhu, H. S. Chae, T. Van Voorhis, M. A. Baldo and T. M. Swager, *J. Am. Chem. Soc.*, 2015, **137**, 11908–11911.
8 E. Spuling, N. Sharma, I. D. W. Samuel, E. Zysman-Colman and S. Bräse, *Chem. Commun.*, 2018, **54**, 9278–9281.
9 A. Pershin, D. Hall, V. Lemaur, J. C. Sancho-Garcia, L. Muccioli, E. Zysman-Colman, D. Beljonne and Y. Olivier, *Nat. Commun.*, 2019, **10**, 3–7.
10 H. Kaji, H. Suzuki, T. Fukushima, K. Shizu, K. Suzuki, S. Kubo, T. Komino, H. Oiwa, F. Suzuki, A. Wakamiya, Y. Murata and C. Adachi, *Nat. Commun.*, 2015, **6**, 2–9.
11 D. H. Ahn, S. W. Kim, H. Lee, I. J. Ko, D. Karthik, J. Y. Lee and J. H. Kwon, *Nat. Photonics*, 2019, **13**, 540–546.
12 X. Wang, S. Wang, J. Lv, S. Shao, L. Wang, X. Jing and F. Wang, *Chem. Sci.*, 2019, **10**, 2915–2923.
13 J. Lu, Y. Zheng and J. Zhang, *RSC Adv.*, 2015, **5**, 18588–18592.
14 L. Gan, Z. Xu, Z. Wang, B. Li, W. Li, X. Cai, K. Liu, Q. Liang and S. J. Su, *Adv. Funct. Mater.*, 2019, **29**, 1808088.
15 X. Liang, Z. L. Tu and Y. X. Zheng, *Chem. – Eur. J.*, 2019, **25**, 5623–5642.
16 T. Hatakeyama, K. Shiren, K. Nakajima, S. Nomura, S. Nakatsuka, K. Kinoshita, J. Ni, Y. Ono and T. Ikuta, *Adv. Mater.*, 2016, **28**, 2777–2781.
17 X. Liang, Z. P. Yan, H. B. Han, Z. G. Wu, Y. X. Zheng, H. Meng, J. L. Zuo and W. Huang, *Angew. Chem., Int. Ed.*, 2018, **57**, 11316–11320.
18 S. Madayanad Suresh, D. Hall, D. Beljonne, Y. Olivier and E. Zysman-Colman, *Adv. Funct. Mater.*, 2020, 1908677.
19 K. M. O. Nuyken, S. Jungermann, V. Wiederhirn and E. Bacher, *Monatsh. Chem.*, 2006, **137**, 811–824.
20 M. Singh, H. M. Haverinen, P. Dhagat and G. E. Jabbour, *Adv. Mater.*, 2010, **22**, 673–685.
21 D. V. A. Arjona-Esteban, *Highly Efficient OLEDs: Materials Based on Thermally Activated Delayed Fluorescence*, 2018, pp. 543–572.
22 L. Duan, L. Hou, T. W. Lee, J. Qiao, D. Zhang, G. Dong, L. Wang and Y. Qiu, *J. Mater. Chem.*, 2010, **20**, 6392–6407.
23 T. Huang, W. Jiang and L. Duan, *J. Mater. Chem. C*, 2018, **6**, 5577–5596.
24 Y. Zou, S. Gong, G. Xie and C. Yang, *Adv. Opt. Mater.*, 2018, **6**, 1–25.
25 J. L. Wu, Y. T. Lee, C. T. Chen and C. T. Chen, *J. Chin. Chem. Soc.*, 2018, **65**, 87–106.
26 C. Li, Z. Ren, X. Sun, H. Li and S. Yan, *Macromolecules*, 2019, **52**, 2296–2303.
27 J. Hu, Q. Li, S. Shao, L. Wang, X. Jing and F. Wang, *Adv. Opt. Mater.*, 2020, 1902100.
28 J. Rao, X. Liu, X. Li, L. Yang, L. Zhao, S. Wang, J. Ding and L. Wang, *Angew. Chem., Int. Ed.*, 2020, **59**, 1320–1326.
29 A. Menon, H. Dong, Z. I. Niazimbetova, L. J. Rothberg and M. E. Galvin, *Chem. Mater.*, 2002, **14**, 3668–3675.
30 Q. Wei, Z. Ge and B. Voit, *Macromol. Rapid Commun.*, 2019, **40**, 1800570.
31 B. Zhang and Y. Cheng, *Chem. Rec.*, 2019, **19**, 1624–1643.
32 T. Jiang, Y. Liu, Z. Ren and S. Yan, *Polym. Chem.*, 2020, **11**, 1555–1571.
33 Y. J. Cho, K. S. Yook and J. Y. Lee, *Adv. Mater.*, 2014, **26**, 6642–6646.
34 X. L. Chen, J. H. Jia, R. Yu, J. Z. Liao, M. X. Yang and C. Z. Lu, *Angew. Chem., Int. Ed.*, 2017, **56**, 15006–15009.
35 Y. Wada, K. Shizu, S. Kubo, K. Suzuki, H. Tanaka, C. Adachi and H. Kaji, *Appl. Phys. Lett.*, 2015, **107**, 183303.
36 Y. Wada, S. Kubo and H. Kaji, *Adv. Mater.*, 2018, **30**, 1705641.
37 J. Lee, K. Shizu, H. Tanaka, H. Nomura, T. Yasuda and C. Adachi, *J. Mater. Chem. C*, 2013, **1**, 4599–4604.
38 Z. Yang, Z. Mao, Z. Xie, Y. Zhang, S. Liu, J. Zhao, J. Xu, Z. Chi and M. P. Aldred, *Chem. Soc. Rev.*, 2017, **46**, 915–1016.
39 Y. Im, M. Kim, Y. J. Cho, J. A. Seo, K. S. Yook and J. Y. Lee, *Chem. Mater.*, 2017, **29**, 1946–1963.
40 O. E. K. A. Hofmann, *Ber. Dtsch. Chem. Ges.*, 1911, **44**, 2713–2717.
41 O. E. K. A. Hofmann, *Ber. Dtsch. Chem. Ges.*, 1912, **45**, 2731–2740.
42 D. W. Kaiser, G. A. Peters and V. P. Wystrach, *J. Org. Chem.*, 1953, **18**, 1610–1615.
43 R. Huisgen, *Chem. Ber.*, 1961, **94**, 1555–1562.
44 R. Cristiano, H. Gallardo, A. J. Bortoluzzi, I. H. Bechtold, C. E. M. Campos and R. L. Longo, *Chem. Commun.*, 2008, 5134–5136.
45 S. K. Pathak, Y. Xiang, M. Huang, T. Huang, X. Cao, H. Liu, G. Xie and C. Yang, *RSC Adv.*, 2020, **10**, 15523–15529.
46 S. Wang, X. Wang, K. H. Lee, S. Liu, J. Y. Lee, W. Zhu and Y. Wang, *Dyes Pigm.*, 2020, **182**, 108589.
47 A. G. Dal-Bó, G. G. L. Cisneros, R. Cercena, J. Mendes, L. M. da Silveira, E. Zapp, K. G. Domiciano, R. da Costa Duarte, F. S. Rodembusch and T. E. A. Frizon, *Dyes Pigm.*, 2016, **135**, 49–56.
48 S. Grimme, *Chem. Phys. Lett.*, 1996, **259**, 128–137.
49 V. Adamo and C. Barone, *J. Chem. Phys.*, 1999, **110**, 6158–6170.
50 T. H. Dunning, *J. Chem. Phys.*, 1989, **90**, 1007–1023.
51 P. L. Santos, J. S. Ward, P. Data, A. S. Batsanov, M. R. Bryce, F. B. Dias and A. P. Monkman, *J. Mater. Chem. C*, 2016, **4**, 3815–3824.
52 T. Hosokai, H. Matsuzaki, H. Nakanotani, K. Tokumaru, T. Tsutsui, A. Furube, K. Nasu, H. Nomura, M. Yahiro and C. Adachi, *Sci. Adv.*, 2017, **3**, 1603282.
53 H. Noda, H. Nakanotani and C. Adachi, *Sci. Adv.*, 2018, **4**, 1–8.
54 P. K. Samanta, D. Kim, V. Coropceanu and J. L. Brédas, *J. Am. Chem. Soc.*, 2017, **139**, 4042–4051.

55 N. Sharma, E. Spuling, C. M. Mattern, W. Li, O. Fuhr, Y. Tsuchiya, C. Adachi, S. Bräse, I. D. W. Samuel and E. Zysman-Colman, *Chem. Sci.*, 2019, **10**, 6689–6696.
56 D. Chen, P. Rajamalli, F. Tenopala-Carmona, C. L. Carpenter-Warren, D. B. Cordes, C. M. Keum, A. M. Z. Slawin, M. C. Gather and E. Zysman-Colman, *Adv. Opt. Mater.*, 2020, **8**, 1901283.
57 P. L. Dos Santos, D. Chen, P. Rajamalli, T. Matulaitis, D. B. Cordes, A. M. Z. Slawin, D. Jacquemin, E. Zysman-Colman and I. D. W. Samuel, *ACS Appl. Mater. Interfaces*, 2019, **11**, 45171–45179.
58 Z. Li, W. Li, C. Keum, E. Archer, B. Zhao, A. M. Z. Slawin, W. Huang, M. C. Gather, I. D. W. Samuel and E. Zysman-Colman, *J. Phys. Chem. C*, 2019, **123**, 24772–24785.
59 M. Y. Wong, S. Krotkus, G. Copley, W. Li, C. Murawski, D. Hall, G. J. Hedley, M. Jaricot, D. B. Cordes, A. M. Z. Slawin, Y. Olivier, D. Beljonne, L. Muccioli, M. Moral, J. C. Sancho-Garcia, M. C. Gather, I. D. W. Samuel and E. Zysman-Colman, *ACS Appl. Mater. Interfaces*, 2018, **10**, 33360–33372.
60 G. A. Crosby and J. N. Demas, *J. Phys. Chem.*, 1971, **75**, 991–1024.